NANO LETTERS

pubs.acs.org/NanoLett

Letter

Carrier-Envelope-Phase Modulated Currents in Scanning Tunneling Microscopy

Ziyang Hu, YanHo Kwok, GuanHua Chen,* and Shaul Mukamel*

Cite This: *Nano Lett.* 2021, 21, 6569−6575

Read Online

ACCESS | Metrics & More | Article Recommendations | Supporting Information

ABSTRACT: Carrier-envelope-phase (CEP) stable optical pulses combined with state-of-the-art scanning tunneling microscopy (STM) can track and control ultrafast electronic tunneling currents. On the basis of nonequilibrium Green's function formalism, we present a time and frequency domain theoretical study of CEP-stable pulse-induced tunneling currents between an STM tip and a metal substrate. It is revealed that the experimentally observed phase shift between the maximum tunneling current and maximum electric field is caused by the third-order response to the electric field. The shift is also found to be sensitive to the duration of pulses. The tunneling process can thus be precisely manipulated by varying the phase and duration of these pulses.

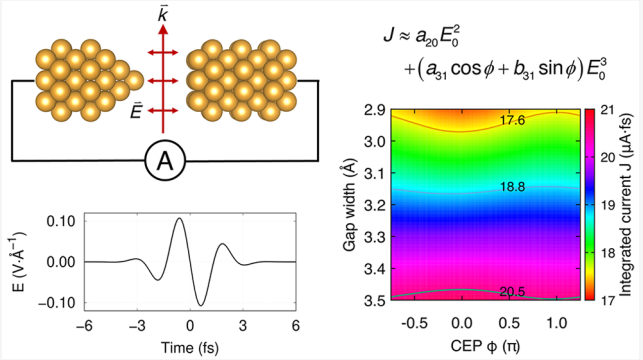

KEYWORDS: *scanning tunneling microscopy, carrier-envelope phase, phase shift, perturbative nonequilibrium Green's functions, tunneling control*

Controlling the ultrafast electron dynamics in nanodevices is one of the central goals of nanoscience. Terahertz (THz) pulses coupled to STM have been recently used to monitor tunneling dynamics with subpicosecond temporal and nanometer spatial resolutions.[1−6] However, THz pulses are too long to track the electron dynamics in its natural femtosecond time scale.[7,8] Ultrashort optical pulses provide a promising route to modulate and track the tunneling process.[9] The electron tunneling was found sensitive to the CEP of the optical pulse.[10−13] Experimentally, the CEP can be precisely modulated and has been used to coherently control the light-driven tunneling current between STM tip and substrate[4,9] and the photoemission of electrons from nanotips.[14,15] Understanding the mechanism of CEP-dependent tunneling current in a junction is thus crucial for advancing ultrafast STM techniques.

The optical pulses created by mode-locked lasers consist of a train of Gaussian enveloped sinusoidal pulses.[9] The vector potential of a laser pulse can be expressed as

$$A(t) = \frac{E_0}{\omega_0} e^{-t^2/2\sigma^2} \cos(\omega_0 t + \phi) \tag{1}$$

Here E_0 is the electric field amplitude, ω_0 is the central frequency, σ is the variance, and ϕ is the CEP, respectively. The full width at half-maximum of the pulse is fwhm $= 2\sqrt{2\ln 2}\,\sigma$. The electric field $E(t) = -\partial_t A(t)$ is an AC field. The CEP is related to the time difference between the peaks of the envelope and the sinusoidal wave as $\Delta t = \phi/\omega_0$. This is controlled by attosecond technology.[16−24] The vector potential and CEP are illustrated in Figure 1a. The electric field variation with the CEP is shown in Figure 1b.

Detecting the femtosecond transient tunneling current in real time is not possible with current technology. The quantity being measured is the average current during a pulse period, i.e., the integrated current.[5,9] The electric field changes with the CEP, and the measured tunneling current will vary as well. However, the measured tunneling current is not synchronous with the electric field but has a phase shift.[1,4,9] To study the role of the phase shift, we first derive perturbative expressions in the optical field for the integrated current based on nonequilibrium Green's function (NEGF) formalism[25,26] and then verify them by time-domain nonperturbative[27−29] and perturbative[30] simulations.

Consider an STM junction coupled to two leads, i.e., tip and substrate with noninteracting electrons. The time-dependent current passing through each lead can be expressed based on Keldysh NEGF formalism as[31]

$$I_\alpha(t) = e\int d\tau \mathrm{tr}[\mathbf{G}^<(t,\tau)\Sigma_\alpha^a(\tau,t) + \mathbf{G}^r(t,\tau)\Sigma_\alpha^<(\tau,t) + \mathrm{hc}] \tag{2}$$

Received: May 15, 2021
Revised: July 19, 2021
Published: July 23, 2021

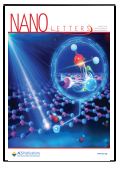

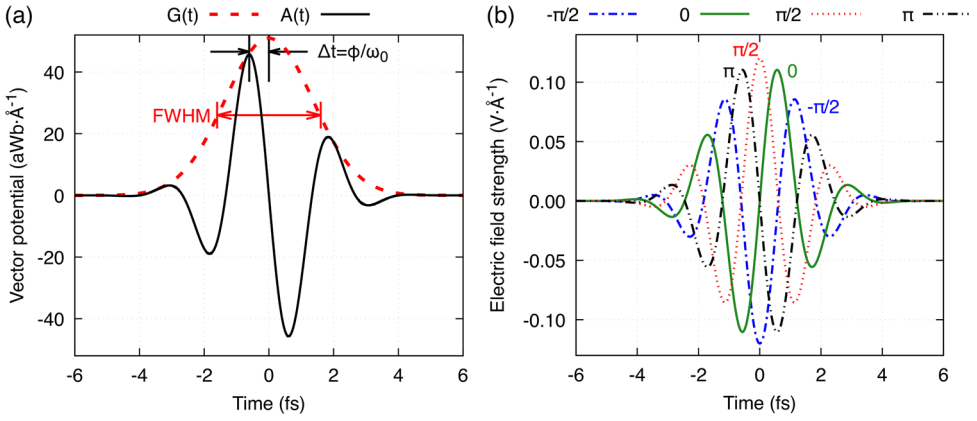

Figure 1. (a) One of the vector potentials used in our simulations. Red dotted line: the Gaussian envelope $G(t)$ with an fwhm of 3.2 fs and an amplitude of 51.0 aWb/Å; black solid line: the vector potential $A(t)$ with a central frequency equivalent to 1.55 eV (800 nm) and a CEP of 0.5 π. The time difference between the peaks of the envelope and the sinusoidal wave is $\Delta t = \phi/\omega_0$. (b) The electric field variation with the CEP.

Here $\mathbf{G}^{<\mathrm{r}}$ is the lesser/retarded Green's function, and $\Sigma_\alpha^{a/<}$ is the advanced/lesser self-energy of lead α, respectively. Because the tunneling gap investigated is relatively narrow, the optical electric field can be approximated as quasi-static.[6] Upon the application of an electric field, the induced bias at each lead can thus be taken as $V_\alpha(t) = \pm E(t)L/2$. Here $E(t)$ is the near-field strength determined by eq 1, and L is the device region length along the transport direction. Since the applied electric field wavelength is much longer than the device size, the amplitude E_0 can be considered to be constant within the system of interest. The potential will be almost flat inside the tip and substrate, owing to screening, and the potential drops between the gap, inducing the local field enhancement. The coupling Hamiltonian to the electric field is $\Delta\ (t) = -\mu E(t)$ within dipole approximation, where μ is the electric dipole moment matrix of the device region. The variations of Green's function and self-energy with the electric field are induced by both the bias and Hamiltonian changes. In the wide-band limit approximation,[32] the advanced self-energy is invariant to the external voltage, and the n-th order response of lesser self-energy can be expressed as[33]

$$\Sigma_n^<(t,\tau) = \frac{1}{n!}\left[\frac{i}{\hbar}\int_t^\tau \mathrm{d}t' eV(t')\right]^n \Sigma_0^<(t,\tau) \tag{3}$$

The n-th order variations of the retarded and lesser Green's functions are then[34]

$$\mathbf{G}_n^r(t, t_{n+1}) = \int \mathrm{d}t_1 \cdots \mathrm{d}t_n \mathbf{G}_0^r(t, t_1) \prod_{j=1}^{n} \Delta(t_j)\mathbf{G}_0^r(t_j, t_{j+1}) \tag{4}$$

$$\mathbf{G}_n^<(t,\tau) = \sum_{i=0,j=0,k=0}^{i+j+k=n} \int \mathrm{d}t_1 \mathrm{d}t_2 \mathbf{G}_i^r(t, t_1)\Sigma_j^<(t_1, t_2)\mathbf{G}_k^a(t_2, \tau) \tag{5}$$

$\Sigma^<$ is the sum of self-energies of all leads. Thus, the n-th order response current is

$$I_\alpha^{(n)}(t) = e\int \mathrm{d}\tau \mathrm{tr}\left[\mathbf{G}_n^<(t,\tau)\Sigma_\alpha^a(\tau, t) + \sum_{i=0,j=0}^{i+j=n} \mathbf{G}_i^r(t,\tau)\Sigma_{\alpha_j}^<(\tau, t) + \mathrm{hc}\right] \tag{6}$$

The integrated current is

$$J_\alpha^{(n)} = \int \mathrm{d}t I_\alpha^{(n)}(t) \tag{7}$$

It is more convenient to work on frequency domain whereby

$$J_\alpha^{(n)} = I_\alpha^{(n)}(\omega = 0) \tag{8}$$

It is straightforward to get the integrated first-order response current as[31]

$$J_\alpha^{(1)} = \frac{eE(\omega=0)}{2\pi\hbar}\sum_\beta \int \mathrm{d}\varepsilon \mathrm{tr}[\mathcal{G}_{\alpha\beta}^{(1)}(\varepsilon)] \tag{9}$$

$\mathcal{G}_{\alpha\beta}^{(1)}$ is given in Supporting Information. The integrated electric field is given by

$$E(\omega=0) = \frac{i\omega}{\omega_0}(\sqrt{2\pi}e^{-\sigma^2\omega_0^2/2}\sigma\cos\phi)E_0\Big|_{\omega=0} = 0 \tag{10}$$

We, therefore, obtain the zero first-order integrated current

$$J_\alpha^{(1)} = 0 \tag{11}$$

Thus, phase control is impossible in the linear response.[35,36] Similarly, for the second-order integrated current, we have

$$J_\alpha^{(2)} = \frac{e}{4\pi^2\hbar^2}\sum_\beta \int \mathrm{d}\varepsilon_1 E(-\varepsilon_1/\hbar)E(\varepsilon_1/\hbar)\int \mathrm{d}\varepsilon \mathrm{tr}[\mathcal{G}_{\alpha\beta}^{(2)}(\varepsilon, \varepsilon_1)] \tag{12}$$

$\mathcal{G}_{\alpha\beta}^{(2)}(\varepsilon, \varepsilon_1)$ is given in Supporting Information. For the electric field part, we obtain

$$E(-\varepsilon_1/\hbar)E(\varepsilon_1/\hbar) = \left(\frac{\varepsilon_1\sigma E_0}{\hbar\omega_0}\right)^2 \pi e^{-\sigma^2[\omega_0^2+(\varepsilon_1/\hbar)^2]}[\cos(2\phi) + \cosh(2\sigma^2\omega_0\varepsilon_1/\hbar)] \tag{13}$$

Denoting the coefficients before E_0^2 as a_{20} and $\cos\ (2\phi)\ E_0^2$ as a_{22}, respectively, we have

$$J_\alpha^{(2)} = [a_{20} + a_{22}\cos(2\phi)]E_0^2 \tag{14}$$

Experimental $\hbar\omega_0$ is around several eV, and $\sigma/\hbar$ is around several eV^{-1}, thus $\cosh\ (2\sigma^2\omega_0\varepsilon_1/\ \hbar) \gg 1$ for not too small ε_1. Consequently, we have $a_{20} \gg a_{22}$; i.e., $J_a^{(2)} \approx a_{20}\ E_0^2$. The second-order response thus acts as a rectifier for all ϕ.

The third-order integrated current is

$$J_\alpha^{(3)} = \frac{e}{8\pi^3\hbar^3}\sum_\beta \iint \mathrm{d}\varepsilon_2 \mathrm{d}\varepsilon_1 E\left(\frac{\varepsilon_1}{\hbar}\right)E\left(\frac{\varepsilon_2-\varepsilon_1}{\hbar}\right)E\left(-\frac{\varepsilon_2}{\hbar}\right) \int \mathrm{d}\varepsilon \mathrm{tr}[\mathcal{G}_{\alpha\beta}^{(3)}(\varepsilon, \varepsilon_1, \varepsilon_2)] \tag{15}$$

https://doi.org/10.1021/acs.nanolett.1c01900
Nano Lett. 2021, 21, 6569−6575

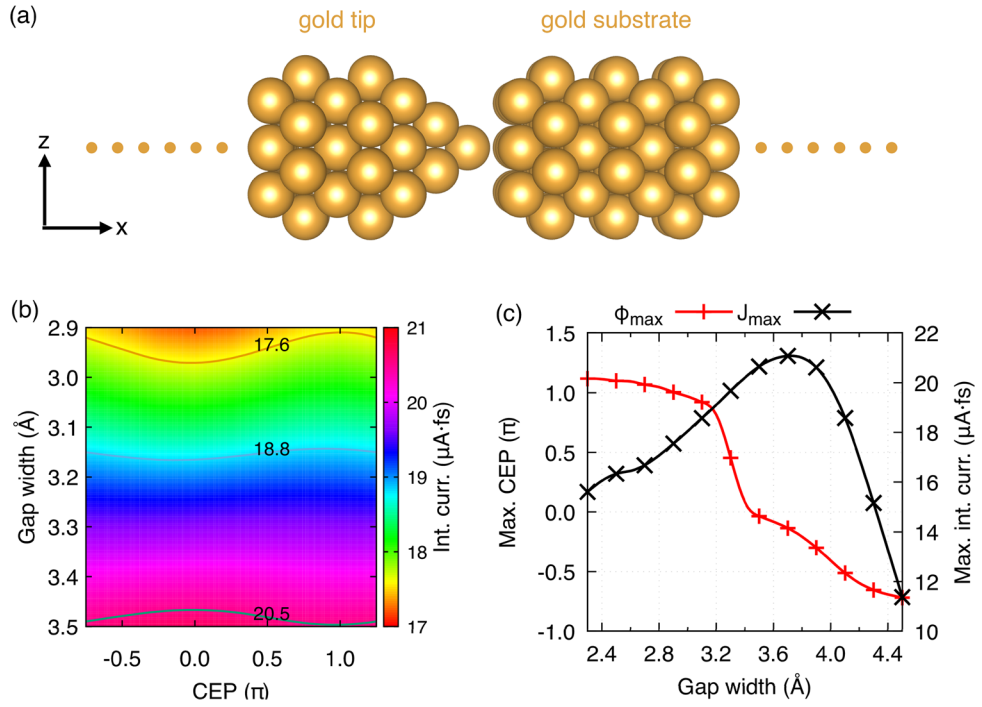

Figure 2. CEP modulated tunneling in a gold-tip-gold-substrate system. (a) The structure of the device region used in TDDFTB-OS simulations. Both the tip and substrate are semi-infinite in the $-x/+x$-directions, respectively. (b) Modulated integrated current as a function of CEP and gap width. The color bar displays the integrated current in μA fs. Three contours are plotted to guide the eyes of readers to the maxima of integrated current. The applied electric field is transmitted along the z-direction and polarized along the x-direction. E_0 = 0.05 V/Å, $\hbar\omega_0$ = 1.55 eV (800 nm), and fwhm = 3.4 fs. (c) The maximum integrated current (J_{max}) and the corresponding CEP (ϕ_{max}) as a function of gap width. ϕ_{max} is plotted as the red "+" line with scales at the left vertical axis. J_{max} is plotted as the black "×" line with scales at the right vertical axis.

The electric field part is

$$E\left(\frac{\varepsilon_1}{\hbar}\right)E\left(\frac{\varepsilon_2-\varepsilon_1}{\hbar}\right)E\left(-\frac{\varepsilon_2}{\hbar}\right)$$
$$=\left(\frac{\sigma E_0}{\hbar\omega_0}\right)^3\pi\sqrt{\frac{\pi}{2}}\varepsilon_1(\varepsilon_2-\varepsilon_1)\varepsilon_2 e^{-\sigma^2[(\varepsilon_1^2-\varepsilon_1\varepsilon_2+\varepsilon_2^2)/\hbar^2+3\omega_0^2/2]}$$
$$[iA\cos\phi - B\sin\phi + \cos(3\phi)] \tag{16}$$

where

$$A = \cosh(2\sigma^2\omega_0\varepsilon_1/\hbar) + \cosh[2\sigma^2\omega_0(\varepsilon_1-\varepsilon_2)/\hbar] + \cosh(2\sigma^2\omega_0\varepsilon_2/\hbar)$$
$$B = \sinh(2\sigma^2\omega_0\varepsilon_1/\hbar) - \sinh[2\sigma^2\omega_0(\varepsilon_1-\varepsilon_2)/\hbar] - \sinh(2\sigma^2\omega_0\varepsilon_2/\hbar) \tag{17}$$

$\mathcal{G}^{(3)}_{\alpha\beta}(\varepsilon, \varepsilon_1, \varepsilon_2)$ is given in Supporting Information. We thus have

$$J^{(3)}_\alpha = [a_{31}\cos\phi + b_{31}\sin\phi + a_{33}\cos(3\phi)]E_0^3 \tag{18}$$

With the same argument, we have $a_{31}, b_{31} \gg a_{33}$.

The integrated current to third order in the optical field is thus given by

$$J_\alpha \approx a_{20}E_0^2 + a_{31}E_0^3\cos\phi + b_{31}E_0^3\sin\phi$$
$$= a_{20}E_0^2 + R\cos(\phi-\phi_{max})E_0^3 \tag{19}$$

where

$$R = \sqrt{a_{31}^2 + b_{31}^2}$$
$$\tan\phi_{max} = b_{31}/a_{31} \tag{20}$$

Here ϕ_{max} is the CEP that maximizes the integrated current. It is apparent that the ϕ_{max} is mainly caused by the third-order response. Note that a_{20}, a_{31}, and b_{31} are not solely determined by the system but are also related to the central frequency and fwhm of the external electric field.

To examine further, we carry out a quantum mechanical simulation of a gold-tip-gold-substrate system using the open system time-dependent density-functional tight-binding (TDDFTB-OS) method.[27−29] Both the tip and substrate are semi-infinite along the transmission direction x. The device region containing 128 gold atoms is depicted in Figure 2a, with the gap width varying from 2.3 to 4.5 Å. The Gaussian pulse with an amplitude of 0.05 V/Å is transmitted along z and polarized along x. The central frequency is 1.55 eV (800 nm) with an fwhm of 3.4 fs. The wide-band limit approximation is applied, and the induced Hamiltonian $\Delta(t)$ is obtained by solving the Poisson equation. DFTB parameters provided by A. Fihey et al. are used.[37] The system is propagated up to 160 fs with the applied electric field. The integrated current (J) containing the response to all orders with different gap widths and CEP is plotted in Figure 2b. ϕ_{max} and the corresponding maximum integrated current (J_{max}) at each gap width are depicted in Figure 2c. J_{max} has a peak near a gap width of 3.7 Å. When the gap width is small, the tip and substrate fuse into a single metal and thus screen out the electric field.[38] From Figure 2c, it is clear that ϕ_{max} changes with the gap width monotonically, which is consistent with the experimental results.[9]

https://doi.org/10.1021/acs.nanolett.1c01900
Nano Lett. 2021, 21, 6569−6575

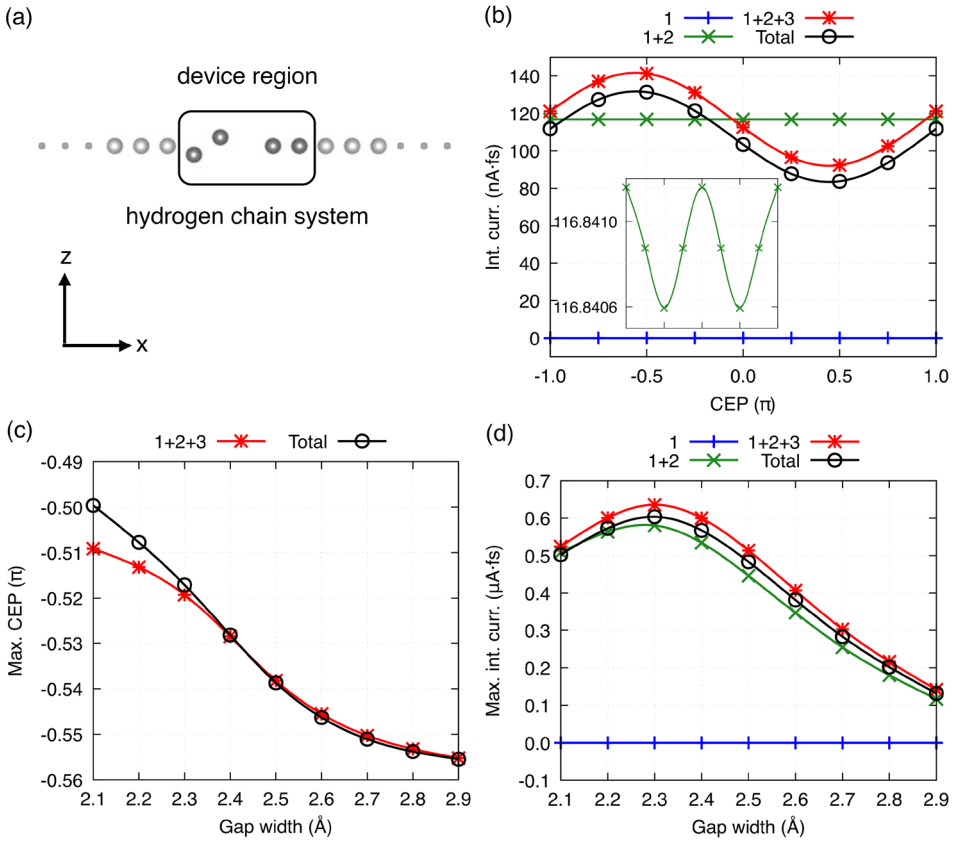

Figure 3. Perturbative time-domain simulation of a hydrogen chain system. (a) The chain structure. The device region included in the TDDFTB-OS simulation is framed by the black rounded rectangle. Both leads are semi-infinitely extended to the $-x/+x$-directions. (b) The sum of different orders integrated current as a function of CEP at a gap width of 2.9 Å. (c) The maximum CEP calculated from the sum of different orders integrated current as a function of gap width. (d) The maximum integrated current calculated from the sum of different orders responses as a function of gap width. The first-order integrated current $J^{(1)}$, the sum of first- and second-order integrated current $J^{(1)}+J^{(2)}$, the sum of first-, second-, third-order integrated current $J^{(1)}+J^{(2)}+J^{(3)}$, and full-order integrated current J are plotted as blue "+", green "×", red "*", and black "○" lines, respectively.

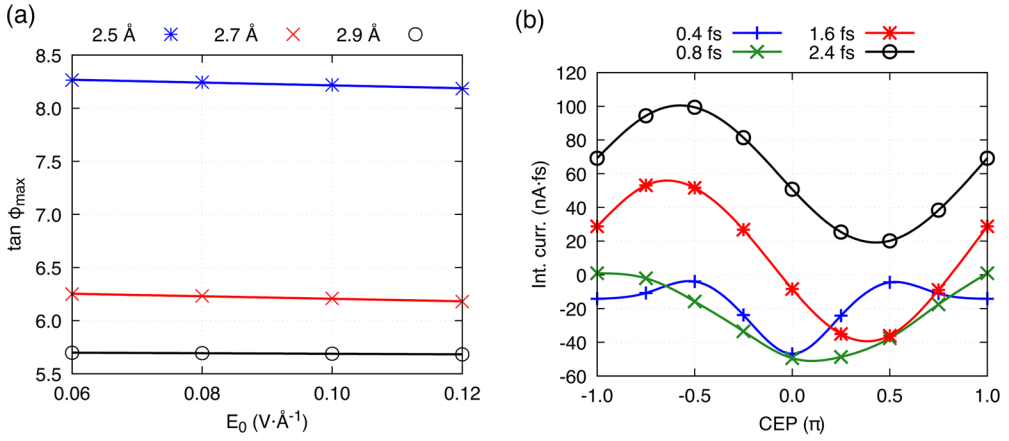

Figure 4. (a) The relation between the tangent of maximum CEP (tan ϕ_{max}) and the amplitude of electric field (E_0). ϕ_{max} calculated from the hydrogen chain system depicted in Figure 3a at gap widths of 2.5, 2.7, and 2.9 Å are plotted as the blue "*", red "×", and black "○" marks, respectively. The solid lines are the linearly fitted curves. (b) Total integrated current with pulses of different fwhm for the hydrogen chain system at gap width 2.9 Å. The minimum of integrated current shifts to 0 π as fwhm decreases.

To verify the frequency-domain analysis, which implies that the shift of ϕ_{max} is at least a third-order effect, we have performed a time-domain perturbative TDDFTB-OS simulation[30] for the asymmetric hydrogen chain system shown in Figure 3a. Simulating the order-by-order dynamics of the gold−gold system is too expensive. The hydrogen chain system is chosen to demonstrate our point. The device region contains 4 hydrogen atoms with the gap width varying between 2.1 and 2.9 Å. The distance between hydrogen atoms on each side is 1.5 Å along x. The Gaussian pulse with an amplitude of 0.12 V/Å is transmitted along z and polarized along the transmission direction (x). The central frequency is 1.55 eV

https://doi.org/10.1021/acs.nanolett.1c01900
Nano Lett. 2021, 21, 6569−6575

(800 nm) with an fwhm of 3.2 fs. DFTB parameters were provided by M. Elstner et al.[39] A 29 fs simulation was required to get the saturated integrated current. In Figure 3b, we analyze the maximum integrated current calculated by the sum of different orders responses as a function of the CEP at a gap width of 2.9 Å. $J^{(1)}$ is zero within numerical errors, and $J^{(2)}$ increases the integrated current almost homogeneously for all CEP. The inset shows the negligible variation of $J^{(2)}$ with the CEP. $J^{(3)}$ shifts ϕ_{max} to $-0.555\ \pi$, and the higher-order responses do not shift ϕ_{max} further. ϕ_{max} and J_{max} calculated from the sum of different orders responses with various gap widths are plotted separately in Figure 3c,d. Again, only for the sum of first-, second-, and third-order integrated current ϕ_{max} depends on the gap width and is virtually identical to ϕ_{max} obtained from the total nonperturbative integrated current. From Figure 3d, the difference between J_{max} obtained from the sum of first-, second-, and third-order responses and J_{max} from the total responses is negligible. We thus verified that the shift of ϕ_{max} from 0 is at least a third-order effect in the optical field. This is consistent with M. Garg and K. Kern's experimental work,[9] where the shift of ϕ_{max} was observed at a field-driven regime, in which third-order photon processes contribute.

To validate eqs 19 and 20, ϕ_{max} is calculated for different E_0 values, where third-order response dominates using the same time-domain method for the same hydrogen chain system. The relation between tan ϕ_{max} and E_0 is shown in Figure 4a for gap widths of 2.5 Å (blue), 2.7 Å (red), and 2.9 Å (black). The marked points in Figure 4a are the simulated results, while the solid lines are the linearly fitted functions. The lines are almost horizontal; thus, eq 20 is confirmed. At small gap widths, the second-order response cos (2ϕ) is stronger, causing the slight inclination of fitted lines. This relation may further be checked with existing experimental techniques in the future.

For a fixed gap width, ϕ_{max} is also determined by the fwhm of the pulse. We consider two extreme cases where the fwhm tends to zero and infinity. When expanding eqs 13 and 16 at $\sigma = 0$, we have

$$E\left(-\frac{\varepsilon_1}{\hbar}\right)E\left(\frac{\varepsilon_1}{\hbar}\right) = O(\sigma^2)[1 + \cos(2\phi)]$$

$$E\left(\frac{\varepsilon_1}{\hbar}\right)E\left(\frac{\varepsilon_2 - \varepsilon_1}{\hbar}\right)E\left(-\frac{\varepsilon_2}{\hbar}\right) = O(\sigma^3)[3\cos\phi + \cos(3\phi)]$$
$$+[O(\sigma^5)\cos\phi + O(\sigma^9)\sin\phi + O(\sigma^5)\cos(3\phi)] \quad (21)$$

It is clear that cos ϕ and cos (2ϕ) dominate in the integrated current, so ϕ_{max} will be less shifted from 0 for a small fwhm. We simulated the hydrogen chain system with a decreasing fwhm of pulses at a gap width of 2.9 Å using the time-domain method and plotted the results in Figure 4b. It is clear the cos ϕ component becomes more dominant as fwhm decreases, and for a small enough fwhm, the cos (2ϕ) term emerges. For a large fwhm scenario, $E(\varepsilon_1)\ E(\varepsilon_2 - \varepsilon_1)\ E(-\varepsilon_2)$ vanishes, so the integrated current will be independent of the CEP.

We note that the shifted ϕ_{max} is not due to the system's asymmetry. We can still observe the shift $\phi_{max} = 0.6\ \pi$ for a symmetric hydrogen chain with a gap width of 2.9 Å at an electric field amplitude of 0.12 V/Å and an fwhm of 3.2 fs. Instead, asymmetry leads to an even order integrated current and results in the rectifier effect.[40] Especially for a large fwhm, the odd order signal vanishes, and the total integrated current will be virtually independent of the CEP.

If the tip−substrate system is extremely close to the light source, the integrated field might survive.[41] Then, the first-order integrated current will interfere with the third-order integrated current and further shift the ϕ_{max}.

In this work, the wide-band limit approximation is adopted. The inclusion of the electronic structures of the leads will make $\mathcal{G}^{(i)}_{\alpha\beta}$ considerably complicated.[31] For the current in the negative differential resistance regime, the coefficients before cosine and sine terms will change, but our conclusion will still hold.

In summary, time-domain TDDFTB-OS simulations demonstrate that the tunneling current can be modulated by tuning the CEP of few-cycle optical pulses. The phase shift between the current and the field in a gold-tip-gold-substrate system is found to vary monotonically with the gap width. Analytical expressions of the different order integrated current are obtained by perturbative expansion of the effective tunneling current under the wide-band limit approximation. We find that the first-order integrated current is zero, and the third-order integrated current is phase shifted. The even order responses can generate a rectification of STM for asymmetric systems. We have also performed time-domain perturbative simulations and confirmed that the phase shift is mainly caused by the third and possibly higher-order responses. The phase shift further depends on the central frequency and fwhm of the pulses. These findings demonstrate how to modulate the tunneling process by tuning the pulse profile. This perturbative technique can also be applied to the pump−probe setup and will be reported in the future.

■ ASSOCIATED CONTENT

Supporting Information

The Supporting Information is available free of charge at https://pubs.acs.org/doi/10.1021/acs.nanolett.1c01900.

Detailed derivation of first-, second-, and third-order integrated currents in the nonequilibrium Green's function formalism under wide-band limit approximation (PDF)

■ AUTHOR INFORMATION

Corresponding Authors

GuanHua Chen − *Department of Chemistry, The University of Hong Kong, Pokfulam, Hong Kong SAR; Hong Kong Quantum AI Lab Limited, Pak Shek Kok, Hong Kong SAR;* orcid.org/0000-0001-5015-0902; Email: ghc@everest.hku.hk

Shaul Mukamel − *Department of Chemistry and Physics & Astronomy, University of California, Irvine, California 92617, United States;* orcid.org/0000-0002-6015-3135; Email: smukamel@uci.edu

Authors

Ziyang Hu − *Department of Chemistry, The University of Hong Kong, Pokfulam, Hong Kong SAR;* orcid.org/0000-0002-7693-5457

YanHo Kwok − *Department of Chemistry, The University of Hong Kong, Pokfulam, Hong Kong SAR; QuantumFabless Limited, Sha Tin, Hong Kong SAR;* orcid.org/0000-0003-1325-4416

Complete contact information is available at: https://pubs.acs.org/10.1021/acs.nanolett.1c01900

https://doi.org/10.1021/acs.nanolett.1c01900
Nano Lett. 2021, 21, 6569−6575

Notes

The authors declare no competing financial interest.

■ ACKNOWLEDGMENTS

Financial support to Z.H., Y.H.K., and G.H.C. from the RGC General Research Fund under grant no. 17309620 and Hong Kong Quantum AI Lab Limited and to S.M. from the National Science Foundation under grant no. CHE-1953045 is gratefully acknowledged.

■ REFERENCES

(1) Jelic, V.; Iwaszczuk, K.; Nguyen, P. H.; Rathje, C.; Hornig, G. J.; Sharum, H. M.; Hoffman, J. R.; Freeman, M. R.; Hegmann, F. A. Ultrafast Terahertz Control of Extreme Tunnel Currents through Single Atoms on a Silicon Surface. *Nat. Phys.* **2017**, *13* (6), 591−598.

(2) Cocker, T. L.; Peller, D.; Yu, P.; Repp, J.; Huber, R. Tracking the Ultrafast Motion of a Single Molecule by Femtosecond Orbital Imaging. *Nature* **2016**, *539* (7628), 263−267.

(3) Yoshida, S.; Hirori, H.; Tachizaki, T.; Yoshioka, K.; Arashida, Y.; Wang, Z.-H.; Sanari, Y.; Takeuchi, O.; Kanemitsu, Y.; Shigekawa, H. Subcycle Transient Scanning Tunneling Spectroscopy with Visualization of Enhanced Terahertz near Field. *ACS Photonics* **2019**, *6* (6), 1356−1364.

(4) Yoshioka, K.; Katayama, I.; Arashida, Y.; Ban, A.; Kawada, Y.; Konishi, K.; Takahashi, H.; Takeda, J. Tailoring Single-Cycle near Field in a Tunnel Junction with Carrier-Envelope Phase-Controlled Terahertz Electric Fields. *Nano Lett.* **2018**, *18* (8), 5198−5204.

(5) Cocker, T. L.; Jelic, V.; Gupta, M.; Molesky, S. J.; Burgess, J. A. J.; Reyes, G. D. L.; Titova, L. V.; Tsui, Y. Y.; Freeman, M. R.; Hegmann, F. A. An Ultrafast Terahertz Scanning Tunnelling Microscope. *Nat. Photonics* **2013**, *7* (8), 620−625.

(6) Müller, M.; Martín Sabanés, N.; Kampfrath, T.; Wolf, M. Phase-Resolved Detection of Ultrabroadband THz Pulses inside a Scanning Tunneling Microscope Junction. *ACS Photonics* **2020**, *7* (8), 2046−2055.

(7) Goulielmakis, E.; Loh, Z.-H.; Wirth, A.; Santra, R.; Rohringer, N.; Yakovlev, V. S.; Zherebtsov, S.; Pfeifer, T.; Azzeer, A. M.; Kling, M. F.; Leone, S. R.; Krausz, F. Real-Time Observation of Valence Electron Motion. *Nature* **2010**, *466* (7307), 739−743.

(8) Kübel, M.; Dube, Z.; Naumov, A. Y.; Villeneuve, D. M.; Corkum, P. B.; Staudte, A. Spatiotemporal Imaging of Valence Electron Motion. *Nat. Commun.* **2019**, *10* (1), 1042.

(9) Garg, M.; Kern, K. Attosecond Coherent Manipulation of Electrons in Tunneling Microscopy. *Science* **2020**, *367* (6476), 411.

(10) Ludwig, M.; Aguirregabiria, G.; Ritzkowsky, F.; Rybka, T.; Marinica, D. C.; Aizpurua, J.; Borisov, A. G.; Leitenstorfer, A.; Brida, D. Sub-Femtosecond Electron Transport in a Nanoscale Gap. *Nat. Phys.* **2020**, *16* (3), 341−345.

(11) Chen, L.; Zhang, Y.; Chen, G.; Franco, I. Stark Control of Electrons Along Nanojunctions. *Nat. Commun.* **2018**, *9* (1), 2070.

(12) Higuchi, T.; Heide, C.; Ullmann, K.; Weber, H. B.; Hommelhoff, P. Light-Field-Driven Currents in Graphene. *Nature* **2017**, *550* (7675), 224−228.

(13) Garzón-Ramírez, A. J.; Franco, I. Symmetry Breaking in the Stark Control of Electrons at Interfaces (Sceli). *J. Chem. Phys.* **2020**, *153* (4), 044704.

(14) Krüger, M.; Schenk, M.; Hommelhoff, P. Attosecond Control of Electrons Emitted from a Nanoscale Metal Tip. *Nature* **2011**, *475* (7354), 78−81.

(15) Piglosiewicz, B.; Schmidt, S.; Park, D. J.; Vogelsang, J.; Groß, P.; Manzoni, C.; Farinello, P.; Cerullo, G.; Lienau, C. Carrier-Envelope Phase Effects on the Strong-Field Photoemission of Electrons from Metallic Nanostructures. *Nat. Photonics* **2014**, *8* (1), 37−42.

(16) Deng, Y.; Schwarz, A.; Fattahi, H.; Ueffing, M.; Gu, X.; Ossiander, M.; Metzger, T.; Pervak, V.; Ishizuki, H.; Taira, T.; Kobayashi, T.; Marcus, G.; Krausz, F.; Kienberger, R.; Karpowicz, N. Carrier-Envelope-Phase-Stable, 1.2 mJ, 1.5 Cycle Laser Pulses at 2.1 Mm. *Opt. Lett.* **2012**, *37* (23), 4973−4975.

(17) Fuji, T.; Rauschenberger, J.; Gohle, C.; Apolonski, A.; Udem, T.; Yakovlev, V. S.; Tempea, G.; Hänsch, T. W.; Krausz, F. Attosecond Control of Optical Waveforms. *New J. Phys.* **2005**, *7*, 116−116.

(18) Rauschenberger, J.; Fuji, T.; Hentschel, M.; Verhoef, A. J.; Udem, T.; Gohle, C.; Hänsch, T. W.; Krausz, F. Carrier-Envelope Phase-Stabilized Amplifier System. *Laser Phys. Lett.* **2006**, *3* (1), 37−42.

(19) Lücking, F.; Assion, A.; Apolonski, A.; Krausz, F.; Steinmeyer, G. Long-Term Carrier-Envelope-Phase-Stable Few-Cycle Pulses by Use of the Feed-Forward Method. *Opt. Lett.* **2012**, *37* (11), 2076−2078.

(20) Hauri, C. P.; Kornelis, W.; Helbing, F. W.; Heinrich, A.; Couairon, A.; Mysyrowicz, A.; Biegert, J.; Keller, U. Generation of Intense, Carrier-Envelope Phase-Locked Few-Cycle Laser Pulses through Filamentation. *Appl. Phys. B: Lasers Opt.* **2004**, *79* (6), 673−677.

(21) Telle, H. R.; Steinmeyer, G.; Dunlop, A. E.; Stenger, J.; Sutter, D. H.; Keller, U. Carrier-Envelope Offset Phase Control: A Novel Concept for Absolute Optical Frequency Measurement and Ultrashort Pulse Generation. *Appl. Phys. B: Lasers Opt.* **1999**, *69* (4), 327−332.

(22) Thomann, I.; Gagnon, E.; Jones, R. J.; Sandhu, A. S.; Lytle, A.; Anderson, R.; Ye, J.; Murnane, M.; Kapteyn, H. Investigation of a Grating-Based Stretcher/Compressor for Carrier-Envelope Phase Stabilized Fs Pulses. *Opt. Express* **2004**, *12* (15), 3493−3499.

(23) Gagnon, E.; Thomann, I.; Paul, A.; Lytle, A. L.; Backus, S.; Murnane, M. M.; Kapteyn, H. C.; Sandhu, A. S. Long-Term Carrier-Envelope Phase Stability from a Grating-Based, Chirped Pulse Amplifier. *Opt. Lett.* **2006**, *31* (12), 1866−1868.

(24) Sandhu, A. S.; Gagnon, E.; Paul, A.; Thomann, I.; Lytle, A.; Keep, T.; Murnane, M. M.; Kapteyn, H. C.; Christov, I. P. Generation of Sub-Optical-Cycle, Carrier-Envelope-Phase—Insensitive, Extreme-UV Pulses via Nonlinear Stabilization in a Waveguide. *Phys. Rev. A: At., Mol., Opt. Phys.* **2006**, *74* (6), 061803.

(25) Stefanucci, G.; Almbladh, C. O. Time-Dependent Quantum Transport: An Exact Formulation Based on TDDFT. *Europhysics Letters (EPL)* **2004**, *67* (1), 14−20.

(26) Keldysh, L. V. Diagram Technique for Nonequilibrium Processes. *Sov. Phys. JETP* **1965**, *20* (4), 1018−1026.

(27) Zheng, X.; Wang, F.; Yam, C. Y.; Mo, Y.; Chen, G. Time-Dependent Density-Functional Theory for Open Systems. *Phys. Rev. B: Condens. Matter Mater. Phys.* **2007**, *75* (19), 195127.

(28) Zheng, X.; Chen, G.; Mo, Y.; Koo, S.; Tian, H.; Yam, C.; Yan, Y. Time-Dependent Density Functional Theory for Quantum Transport. *J. Chem. Phys.* **2010**, *133* (11), 114101.

(29) Zhang, Y.; Chen, S.; Chen, G. First-Principles Time-Dependent Quantum Transport Theory. *Phys. Rev. B: Condens. Matter Mater. Phys.* **2013**, *87* (8), 085110.

(30) Kwok, Y.; Chen, G.; Mukamel, S. Stm Imaging of Electron Migration in Real Space and Time: A Simulation Study. *Nano Lett.* **2019**, *19* (10), 7006−7012.

(31) Mo, Y.; Zheng, X.; Chen, G.; Yan, Y. Transient Electronic Dynamics of Noninteracting Open Systems Beyond Linear Response. *J. Phys.: Condens. Matter* **2009**, *21* (35), 355301.

(32) Jauho, A.-P.; Wingreen, N. S.; Meir, Y. Time-Dependent Transport in Interacting and Noninteracting Resonant-Tunneling Systems. *Phys. Rev. B: Condens. Matter Mater. Phys.* **1994**, *50* (8), 5528−5544.

(33) Kwok, Y. H.; Xie, H.; Yam, C. Y.; Zheng, X.; Chen, G. H. Time-Dependent Density Functional Theory Quantum Transport Simulation in Non-Orthogonal Basis. *J. Chem. Phys.* **2013**, *139* (22), 224111.

(34) van Leeuwen, R.; Dahlen, N. E.; Stefanucci, G.; Almbladh, C. O.; von Barth, U. Introduction to the Keldysh Formalism. In *Time-Dependent Density Functional Theory*; Marques, M. A. L., Ullrich, C. A.,

https://doi.org/10.1021/acs.nanolett.1c01900
Nano Lett. 2021, 21, 6569−6575

Nogueira, F., Rubio, A., Burke, K., Gross, E. K. U., Eds.; Springer Berlin Heidelberg: Berlin, Heidelberg, 2006; pp 33−59.
(35) Franco, I.; Brumer, P. Laser-Induced Spatial Symmetry Breaking in Quantum and Classical Mechanics. *Phys. Rev. Lett.* **2006**, *97* (4), 040402.
(36) Franco, I.; Brumer, P. Minimum Requirements for Laser-Induced Symmetry Breaking in Quantum and Classical Mechanics. *J. Phys. B: At., Mol. Opt. Phys.* **2008**, *41* (7), 074003.
(37) Fihey, A.; Hettich, C.; Touzeau, J.; Maurel, F.; Perrier, A.; Köhler, C.; Aradi, B.; Frauenheim, T. SCC-DFTB Parameters for Simulating Hybrid Gold-Thiolates Compounds. *J. Comput. Chem.* **2015**, *36* (27), 2075−2087.
(38) Yeyati, A. L.; Flores, F. Photocurrent Effects in the Scanning Tunneling Microscope. *Phys. Rev. B: Condens. Matter Mater. Phys.* **1991**, *44* (16), 9020−9024.
(39) Elstner, M.; Porezag, D.; Jungnickel, G.; Elsner, J.; Haugk, M.; Frauenheim, T.; Suhai, S.; Seifert, G. Self-Consistent-Charge Density-Functional Tight-Binding Method for Simulations of Complex Materials Properties. *Phys. Rev. B: Condens. Matter Mater. Phys.* **1998**, *58* (11), 7260−7268.
(40) Nguyen, H. Q.; Cutler, P. H.; Feuchtwang, T. E.; Huang, Z.; Kuk, Y.; Silverman, P. J.; Lucas, A. A.; Sullivan, T. E. Mechanisms of Current Rectification in an Stm Tunnel Junction and the Measurement of an Operational Tunneling Time. *IEEE Trans. Electron Devices* **1989**, *36* (11), 2671−2678.
(41) Brabec, T.; Krausz, F. Intense Few-Cycle Laser Fields: Frontiers of Nonlinear Optics. *Rev. Mod. Phys.* **2000**, *72* (2), 545−591.

https://doi.org/10.1021/acs.nanolett.1c01900
Nano Lett. 2021, 21, 6569−6575